

# Radiative capture reactions from potential models

C. A. Bertulani\* and V. Guimarães†

\*Department of Physics, Texas A&M University-Commerce, Commerce, TX 75429, USA

†Instituto de Física, Universidade de São Paulo P.O.Box 66318, 05389-970 São Paulo, SP, Brazil

**Abstract.** We show how one can calculate radiative capture cross sections and astrophysical S-factors for nuclei in the mass region  $A < 20$  using potential models. We produce a sizeable list of cases for which the model works well. Useful quantities, such as spectroscopic factors and asymptotic normalization coefficients, are obtained and compared to published data.

**Keywords:** radiative capture, single-particle model, light nuclei

**PACS:** 25.40.Lw, 24.50.+g, 26.20.-f

## POTENTIALS AND WAVEFUNCTIONS

We adopt nuclear potentials of the form

$$V(\mathbf{r}) = V_0(r) + V_S(r) (\mathbf{l} \cdot \mathbf{s}) + V_C(r) \quad (1)$$

where  $V_0(r)$  and  $V_S(r)$  are the central and spin-orbit interactions, respectively, and  $V_C(r)$  is the Coulomb potential of a uniform distribution of charges:

$$V_C(r) = \frac{Z_a Z_b e^2}{r} \quad \text{for } r > R_C, \quad \text{and } V_C(r) = \frac{Z_a Z_b e^2}{2R_C} \left( 3 - \frac{r^2}{R_C^2} \right) \quad \text{for } r < R_C, \quad (2)$$

where  $Z_i$  is the charge number of nucleus  $i = a, b$ .

We use a Woods-Saxon (WS) parameterization to build up the potentials  $V_0(r)$  and  $V_S(r)$ , given by

$$V_0(r) = V_0 f_0(r), \quad V_S(r) = -V_{S0} \left( \frac{\hbar}{m_\pi c} \right)^2 \frac{1}{r} \frac{df_S(r)}{dr}, \quad f_i(r) = \left[ 1 + \exp \left( \frac{r - R_i}{a_i} \right) \right]^{-1}. \quad (3)$$

The spin-orbit interaction in Eq. 3 is written in terms of the pion Compton wavelength,  $\hbar/m_\pi c = 1.414$  fm. The parameters  $V_0$ ,  $V_{S0}$ ,  $R_0$ ,  $a_0$ ,  $R_{S0}$ , and  $a_{S0}$  are chosen to reproduce the ground state energy  $E_B$  (or the energy of an excited state). For this purpose, we define typical values (Table I) for  $V_{S0}$ ,  $R_0$ ,  $a_0$ ,  $R_{S0}$ , and vary only the depth of the central potential,  $V_0$ . A different set of potential depths might be used for continuum states.

The wavefunctions for the nucleon (n) + nucleus (x) system are calculated by solving the radial Schrödinger equation

$$-\frac{\hbar^2}{2m_{nx}} \left[ \frac{d^2}{dr^2} - \frac{l(l+1)}{r^2} \right] u_\alpha(r) + V(r)u_\alpha(r) = E_\alpha u_\alpha(r). \quad (4)$$

**TABLE 1.** Parameters of the single-particle potentials, except for few cases explicitly mentioned in the text.

Parameter	Adopted value
$R_0 = R_{S_0} = R_C$	$r_0(A+1)^{1/3}$ fm
$r_0$	1.25
$a_0 = a_{S_0}$	0.65 fm
$V_{S_0}$	-10 MeV

The nucleon  $n$ , the nucleus  $x$ , and the  $n+x=a$ -system have intrinsic spins labeled by  $s = 1/2$ ,  $I_x$  and  $J$ , respectively. The orbital angular momentum for the relative motion of  $n+x$  is described by  $l$ . It is convenient to couple angular momenta as  $\mathbf{l} + \mathbf{s} = \mathbf{j}$  and  $\mathbf{j} + \mathbf{I}_x = \mathbf{J}$ , where  $\mathbf{J}$  is called the channel spin. In Eq. 1 for  $V$  we use  $\mathbf{s} \cdot \mathbf{l} = [j(j+1) - l(l+1) - 3/4]/2$  and  $\alpha$  in Eq. 4 denotes the set of quantum numbers,  $\alpha_b = \{E_b, l_b, j_b, J_b\}$  for the bound state, and  $\alpha_c = \{E_c, l_c, j_c, J_c\}$  for the continuum states.

The bound-state wavefunctions are normalized to unity,  $\int dr |u_{\alpha_b}(r)|^2 = 1$ , whereas the continuum wavefunctions have boundary conditions at infinity given by

$$u_{\alpha_c}(r \rightarrow \infty) = i \sqrt{\frac{m_{nx}}{2\pi k \hbar^2}} \left[ H_l^{(-)}(r) - S_{\alpha_c} H_l^{(+)}(r) \right] e^{i\sigma_l(E)} \quad (5)$$

where  $S_{\alpha_c} = \exp[2i\delta_{\alpha_c}(E)]$ , with  $\delta_{\alpha_c}(E)$  and  $\sigma_l(E)$  being the nuclear and the Coulomb phase-shifts, respectively. In Eq. 5,  $H_l^{(\pm)}(r) = G_l(r) \pm iF_l(r)$ , where  $F_l$  and  $G_l$  are the regular and irregular Coulomb wavefunctions. For neutrons the Coulomb functions reduce to the usual spherical Bessel functions,  $j_l(r)$  and  $n_l(r)$ . With these definitions, the continuum wavefunctions are normalized as  $\langle u_{E'_c} | u_{E_c} \rangle = \delta(E'_c - E_c) \delta_{\alpha\alpha'}$ .

## RADIATIVE CAPTURE CROSS SECTIONS

### Amplitudes and cross sections

The radiative capture cross sections for  $n+x \rightarrow a + \gamma$  and  $\pi L$  ( $\pi = E, (M)$  =electric (magnetic) L-pole) transitions are calculated with

$$\begin{aligned} \sigma_{EL, J_b}^{\text{d.c.}} &= \frac{(2\pi)^3}{k^2} \left( \frac{E_{nx} + E_b}{\hbar c} \right)^{2L+1} \frac{2(2I_a + 1)}{(2I_n + 1)(2I_x + 1)} \frac{L+1}{L[(2L+1)!!]^2} \sum_{J_c J_c'} (2J_c + 1) \\ &\times \left\{ \begin{matrix} j_c & J_c & I_x \\ J_b & j_b & L \end{matrix} \right\}^2 |\langle l_c j_c || \mathcal{O}_{\pi L} || l_b j_b \rangle|^2, \end{aligned} \quad (6)$$

where  $E_b$  is the binding energy and  $\langle l_c j_c || \mathcal{O}_{\pi L} || l_b j_b \rangle$  is the multipole matrix element. For the electric multipole transitions

$$\langle l_c j_c || \mathcal{O}_{EL} || l_b j_b \rangle = (-1)^{l_b + l_c - j_c + L - 1/2} \frac{eL}{\sqrt{4\pi}} \sqrt{(2L+1)(2j_b+1)} \begin{pmatrix} j_b & L & j_c \\ 1/2 & 0 & -1/2 \end{pmatrix}$$

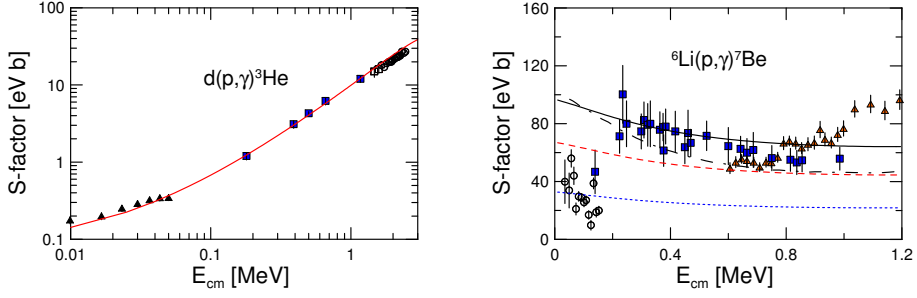


**FIGURE 1.** *Left.* Single-particle model calculation for the reaction  $d(p, \gamma)^3\text{He}$ . Experimental data are from Refs. [2, 3, 4, 5]. The parameters calculated according to Table I are used. The potential depth (here  $V_b = V_c$ ) is given in Table II. *Right.* Single-particle model calculation for the reaction  ${}^6\text{Li}(p, \gamma){}^7\text{Be}$ . The dotted line is the calculation for the capture to the 1st excited of  ${}^7\text{Be}$  and the dashed line for the ground state. The solid line is the total calculated S-factor. Experimental data are from Refs. [6, 7, 8]. The dotted-dashed line is the total S-factor calculated in Ref. [8] using a four-cluster microscopic model.

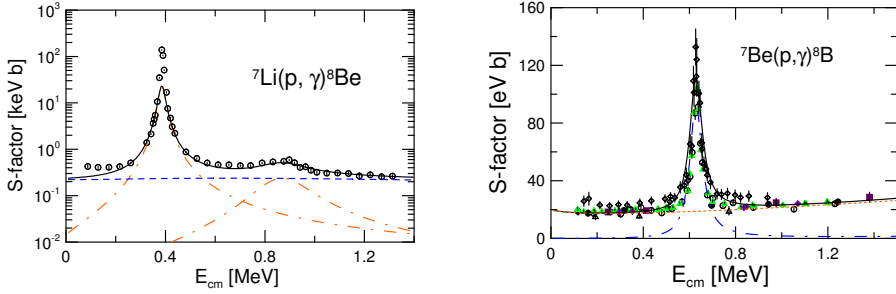


**FIGURE 2.** *Left.* Potential model calculation for the reaction  ${}^7\text{Li}(p, \gamma){}^8\text{Be}$ . Experimental data are from Ref. [9]. *Right.* Single-particle model calculations for the reaction  ${}^7\text{Be}(p, \gamma){}^8\text{B}$ . The dashed-dotted line is the calculation for the M1 resonance at  $E_{cm} = 0.63$  MeV and the dotted line is for the non-resonant capture. Experimental data are from Refs. [10, 11, 12, 13, 14, 15]. The total S factor is shown as a solid line.

$$\times \int_0^\infty dr r^L u_b(r) u_c(r), \quad (7)$$

where  $e_L$  is the effective charge, which takes into account the displacement of the center-of-mass,  $e_L = Z_x e (-m_n/m_a)^L + Z_n e (m_x/m_a)^L$ .

The radiative capture cross sections for  $n+x \rightarrow a + \gamma$  and M1 transitions are calculated with

$$\begin{aligned} \langle l_c j_c \| \mathcal{O}_{M1} \| l_b j_b \rangle = & (-1)^{j_c + I_x + J_b + 1} \sqrt{\frac{3}{4\pi} \mu_N} \left\{ \frac{1}{l_b} e_M \left[ \frac{2\tilde{j}_b}{l_b} (l_b \delta_{j_b, l_b + 1/2} + (l_b + 1) \delta_{j_b, l_b - 1/2}) \right. \right. \\ & \left. \left. + (-1)^{l_b + 1/2 - j_c} \frac{\tilde{j}_b}{\sqrt{2}} \delta_{j_b, l_b \pm 1/2} \delta_{j_c, l_b \mp 1/2} \right] + g_N \frac{1}{l_b^2} \left[ (-1)^{l_b + 1/2 - j_b} \tilde{j}_b \delta_{j_c, j_b} \right. \right. \end{aligned}$$

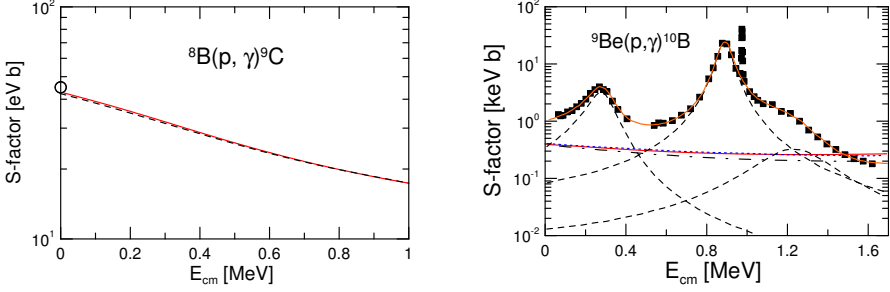


**FIGURE 3.** *Left.* Single-particle model calculations for the reaction  ${}^8\text{B}(p, \gamma){}^9\text{C}$  (solid line). The open circle at  $E = 0$  is from Refs. [16, 17]. The result from Ref. [18] ( $\lambda_{\text{scatt}} = 0.55$  fm) is shown as a dashed line. *Right.* Single-particle model calculations for the reaction  ${}^9\text{Be}(p, \gamma){}^{10}\text{B}$  (solid line). The experimental data are from Ref. [19]. The fits to the resonances, done in Ref. [19], are shown as dashed lines. DC results from Ref. [20] and Ref. [19] are shown as a dotted-dashed line and a dotted line, respectively. The curve passing through the experimental data points is the sum of our DC calculation and the resonance fits, given by the dashed lines.

$$\begin{aligned}
 & - \left( (-1)^{l_b+1/2-j_c} \frac{\hat{j}_b}{\sqrt{2}} \delta_{j_b, l_b \pm 1/2} \delta_{j_c, l_b \mp 1/2} \right) + g_x (-1)^{I_x+j_b+J_c+1} \hat{J}_b \hat{J}_c \hat{I}_x \left\{ \begin{array}{ccc} I_x & J_c & j_b \\ J_b & I_x & 1 \end{array} \right\} \\
 & \times \int_0^\infty dr r u_c(r) u_b(r), \quad (8)
 \end{aligned}$$

where  $\tilde{k} = \sqrt{k(k+1)}$  and  $\hat{k} = \sqrt{2k+1}$ . The spin g-factor is  $g_N = 5.586$  for the proton and  $g_N = -3.826$  for the neutron. The magnetic moment of the core nucleus is given by  $\mu_x = g_x \mu_N$ . If  $l_c \neq l_b$  the magnetic dipole matrix element is zero.

The total direct capture cross section is obtained by adding all multiplicities and final spins of the bound state ( $E \equiv E_{nx}$ ),

$$\sigma^{\text{d.c.}}(E) = \sum_{L, J_b} (SF)_{J_b} \sigma_{L, J_b}^{\text{d.c.}}(E), \quad (9)$$

where  $(SF)_{J_b}$  are spectroscopic factors. For charged particles the astrophysical S-factor for the direct capture from a continuum state to the bound state is defined as

$$S(E) = E \sigma^{\text{d.c.}}(E) \exp[2\pi\eta(E)], \quad \text{with } \eta(E) = Z_a Z_b e^2 / \hbar v, \quad (10)$$

where  $v$  is the initial relative velocity between  $n$  and  $x$ .

For some resonances, not reproducible with the single-particle model, we use a simple Breit-Wigner shape parametrization

$$\sigma_{\text{BW}} = \frac{\Gamma}{2\pi} \frac{\sigma_0(E)}{(E - E_R)^2 + \Gamma^2/4}, \quad (11)$$

where  $E_R$  is the resonance energy. The function  $\sigma_0(E)$  is given by

$$\sigma_0(E) = \frac{\pi \hbar^2}{2m_{xn} E} \frac{2J_R + 1}{(2J_x + 1)(2J_n + 1)} \frac{\Gamma_n(E) \Gamma_\gamma(E)}{\Gamma(E)} \quad (12)$$

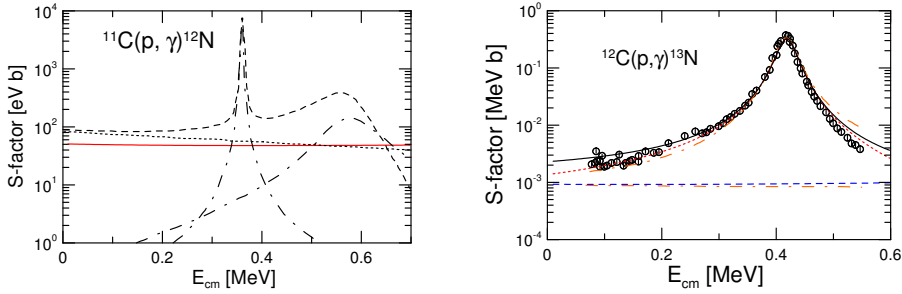


**FIGURE 4.** *Left.* Single-particle model calculations for the reaction  $^{11}\text{C}(p, \gamma)^{12}\text{N}$  (solid line). R-matrix results from Ref. [21] are also shown by dashed lines (resonances) and a dotted line (non-resonant). *Right.* Single-particle model calculations for the reaction  $^{12}\text{C}(p, \gamma)^{13}\text{N}$  are shown as a dashed line (DC), a dotted line ( $E1$  resonance) and a solid line (total). The experimental data are from Ref. [22]. The potential model results from Ref. [23] are shown as dotted-dashed lines.

**TABLE 2.** Binding energy ( $E_b$ , in MeV), central potential depth of bound state ( $V_b$ , in MeV), spectroscopic factor ( $SF$ ), single-particle asymptotic normalization coefficients ( $b$ , in  $\text{fm}^{-1/2}$ ), the factor that multiplies S-factor if the integration in Eq. 6 starts at  $r = R_0$  (nuclear radius) and S-factor at zero energy ( $S(0)$ , in eV b) for radiative proton capture reactions.

Reaction	$E_b$	$V_b$	$SF$	$b$	$> R_0$	$S(0)$
$d(p, \gamma)^3\text{He}$	5.49	-44.43	0.7	1.86	0.98	0.14
$^6\text{Li}(p, \gamma)^7\text{Be}$	5.61	-65.91	0.83 [24]	2.21	1.28	66.8
$^6\text{Li}(p, \gamma)^7\text{Be}^*$	5.18	-64.94	0.84 [8]	2.08	1.19	32.7
$^7\text{Li}(p, \gamma)^8\text{Be}$	17.26	-75.69	1.0	7.84	1.01	238.
$^7\text{Be}(p, \gamma)^8\text{B}$	0.14	-41.26	1.0	0.72	1.00	19.4
$^8\text{B}(p, \gamma)^9\text{C}$	1.30	-41.97	1.0 [18]	1.31	1.08	42.5
$^9\text{Be}(p, \gamma)^{10}\text{B}$	6.59	-49.83	1.0 [25]	3.43	1.27	1052
$^{11}\text{C}(p, \gamma)^{12}\text{N}$	0.60	-40.72	0.4 [26]	1.49	1.01	50.8
$^{12}\text{C}(p, \gamma)^{13}\text{N}$	1.94	-41.65	1.0	2.05	1.04	2346
$^{13}\text{C}(p, \gamma)^{14}\text{N}$	7.55	-50.26	0.33	5.31	1.10	6217
$^{13}\text{N}(p, \gamma)^{14}\text{O}$	4.63	-46.02	1.88 [27]	3.97	1.45	5771
$^{14}\text{N}(p, \gamma)^{15}\text{O}^*$	0.50	-14.83	1.5	4.24	1.00	1470
$^{15}\text{N}(p, \gamma)^{16}\text{O}$	12.13	-54.81	1.8 [28]	10.16	0.78	$2.21 \cdot 10^4$
$^{16}\text{O}(p, \gamma)^{17}\text{F}$	0.60	-49.69	0.9 [29]	0.96	1.02	304
$^{16}\text{O}(p, \gamma)^{17}\text{F}^*$	0.11	-50.70	1.0 [29]	77.21	1.00	9075
$^{20}\text{Ne}(p, \gamma)^{21}\text{Na}^*$	0.006	-47.24	0.7	4.02	1.00	$4.28 \cdot 10^4$
$^{20}\text{Ne}(p, \gamma)^{21}\text{Na}^*$	2.10	-49.63	0.8	2.43	1.00	2493

where the total width  $\Gamma = \Gamma_n + \Gamma_\gamma$  is the sum of the nucleon-decay and the  $\gamma$ -decay widths. For simplicity, and for the cases treated here, we will assume that the resonances are narrow so that  $\sigma_0 = \sigma(E_R)$ .

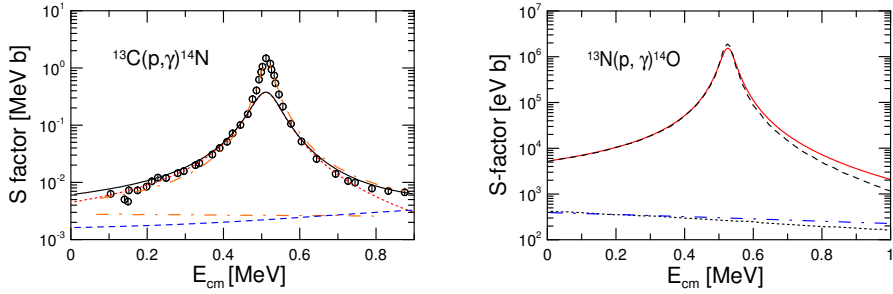


**FIGURE 5.** *Left.* Single-particle model calculations for the reaction  $^{13}\text{C}(p, \gamma)^{14}\text{N}$  are shown as a dashed line (DC), a dotted line ( $E1$  resonance) and a solid line (total). The experimental data are from Ref. [30]. The potential model results from Ref. [23] are shown as dotted-dashed lines. *Right.* Single-particle model calculations for the reaction  $^{13}\text{N}(p, \gamma)^{14}\text{O}$  are shown as a dotted-dashed line (non-resonant) and a solid line ( $E1$  resonance). R-matrix results from Ref. [31] are also shown as a dashed line (resonance) and a dotted line (non-resonant).

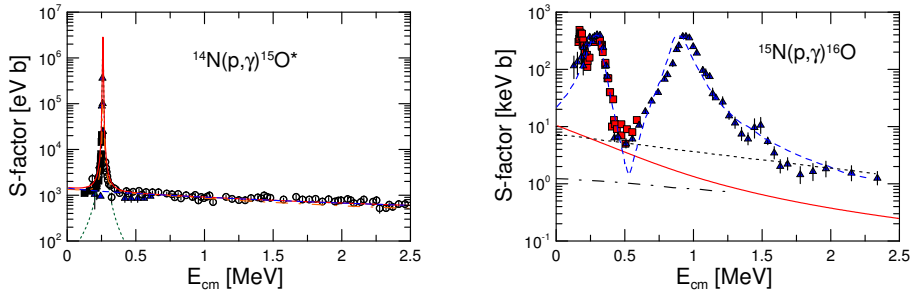


**FIGURE 6.** *Left.* Single-particle model calculations for  $^{14}\text{N}(p, \gamma)^{15}\text{O}$  capture to the 6.793 MeV excited state of  $^{15}\text{O}$ . Dashed line is for the non-resonant capture, dotted line is for the  $M1$  resonance, and the solid line is the total S-factor. The experimental data are from Refs. [32, 33, 34]. The dotted-dashed line is a R-matrix fit obtained in Ref. [32] with the channel radius  $a = 5.5$  fm (this curve is almost invisible because it is very close to our results). *Right.* Single-particle model calculation for the reaction  $^{15}\text{N}(p, \gamma)^{16}\text{O}$  (solid line). The experimental data are from Refs. [28, 35]. Dashed lines are Breit-Wigner fits to the resonances, as described in Ref. [28]. The dotted line is a non-resonant capture of Ref. [28]. The dotted-dashed line represents the non-resonant capture calculation from Ref. [36].

## Asymptotic normalization coefficients

In a microscopic approach, instead of the single-particle wavefunctions one often makes use of overlap integrals,  $I_b(\mathbf{r})$ , and a many-body wavefunction for the relative motion,  $\Psi_c(\mathbf{r})$ . Both  $I_b(\mathbf{r})$  and  $\Psi_c(\mathbf{r})$  might be very complicated to calculate, depending on how elaborated the microscopic model is. The variable  $\mathbf{r}$  is the relative coordinate between the nucleon and the nucleus  $x$ , with all the intrinsic coordinates of the nucleons in  $x$  being integrated out. The direct capture cross sections are obtained from the calculation of  $\sigma_{L, I_b}^{\text{d.c.}} \propto |\langle I_b(r) || r^L Y_L || \Psi_c(r) \rangle|^2$ .

**TABLE 3.** Binding energy ( $E_b$ , in MeV), central potential depth of bound state ( $V_b$ , in MeV), spectroscopic factor ( $SF$ ), single-particle asymptotic normalization coefficients ( $b$ , in  $\text{fm}^{-1/2}$ ) and the factor multiplying the S-factor assuming that the integration in Eq. 6 starts at  $r = R_0$  (nuclear radius).

Reaction	$E_b$	$V_b$	$SF$	$b$	$r > R_0$
$^2\text{H}(n, \gamma)^3\text{H}$	6.26	-44.63	1.0	1.90	0.97
$^7\text{Li}(n, \gamma)^8\text{Li}$	2.03	-43.56	0.87 [37]	0.76	1.04
$^7\text{Li}(n, \gamma)^8\text{Li}^*$	1.05	-40.46	0.48 [37]	0.47	1.02
$^8\text{Li}(n, \gamma)^9\text{Li}$	4.06	-45.29	0.8 [38]	1.25	1.08
$^8\text{Li}(n, \gamma)^9\text{Li}^*$	1.37	-38.57	0.55 [39]	0.54	1.03
$^{11}\text{B}(n, \gamma)^{12}\text{B}$	3.37	-34.33	1.09 [40]	1.35	1.09
$^{12}\text{C}(n, \gamma)^{13}\text{C}$	4.95	-41.35	0.77 [41]	1.85	3.23
$^{12}\text{C}(n, \gamma)^{13}\text{C}^*$	1.86	-56.90	0.8 [42]	1.80	1.00
$^{12}\text{C}(n, \gamma)^{13}\text{C}^*$	1.27	-28.81	0.14 [41]	0.61	1.23
$^{12}\text{C}(n, \gamma)^{13}\text{C}^*$	1.09	-56.85	0.58 [41]	0.15	1.04
$^{14}\text{C}(n, \gamma)^{15}\text{C}$	1.22	-48.63	0.88 [43]	1.44	1.00
$^{15}\text{N}(n, \gamma)^{16}\text{N}$	2.49	-27.06	0.55 [44]	1.14	1.38
$^{15}\text{N}(n, \gamma)^{16}\text{N}^*$	2.37	-12.45	0.46 [44]	1.62	1.11
$^{15}\text{N}(n, \gamma)^{16}\text{N}^*$	2.19	-49.51	0.54 [44]	0.39	2.77
$^{15}\text{N}(n, \gamma)^{16}\text{N}^*$	2.09	-11.90	0.52 [44]	1.50	0.94
$^{16}\text{O}(n, \gamma)^{17}\text{O}$	4.14	-51.77	1.0	0.90	1.17
$^{16}\text{O}(n, \gamma)^{17}\text{O}^*$	3.27	51.60	1.0	3.01	0.99
$^{18}\text{O}(n, \gamma)^{19}\text{O}$	3.96	-47.79	0.69 [45]	0.90	1.17
$^{18}\text{O}(n, \gamma)^{19}\text{O}^*$	3.86	-55.94	0.013 [45]	0.81	1.14
$^{18}\text{O}(n, \gamma)^{19}\text{O}^*$	2.49	-46.33	0.83 [45]	2.48	1.00

The imprints of many-body effects will eventually disappear at large distances between the nucleon and the nucleus. One thus expects that the overlap function asymptotically matches the solution of the Schrödinger equation 4, with  $V = V_C$  for protons and  $V = 0$  for neutrons. That is, when  $r \rightarrow \infty$ ,

$$I_b(r) = C_1 \frac{W_{-\eta, lb+1/2}(2\kappa r)}{r} \text{ for protons, } I_b(r) = C_2 \sqrt{\frac{2\kappa}{r}} K_{lb+1/2}(\kappa r) \text{ for neutrons, (13)}$$

where the binding energy of the  $n + x$  system is related to  $\kappa$  by means of  $E_b = \hbar^2 \kappa^2 / 2m_{nx}$ ,  $W_{p,q}$  is the Whittaker function and  $K_\mu$  is the modified Bessel function. In Eq. 13,  $C_i$  is the asymptotic normalization coefficient (ANC).

In the calculation of  $\sigma_{L,J_b}^{\text{d.c.}}$  above, one often meets the situation in which only the asymptotic part of  $I_b(r)$  and  $\Psi_c(r)$  contributes significantly to the integral over  $r$ . In these situations,  $\Psi_c(r)$  is also well described by a simple two-body scattering wave (e.g. Coulomb waves). Therefore the radial integration in  $\sigma_{L,J_b}^{\text{d.c.}}$  can be done accurately and the only remaining information from the many-body physics at short-distances is contained in the asymptotic normalization coefficient  $C_i$ , i.e.  $\sigma_{L,J_b}^{\text{d.c.}} \propto C_i^2$ . We thus run into an effective theory for radiative capture cross sections, in which the constants  $C_i$  carry all the information about the short-distance physics, where the many-body aspects

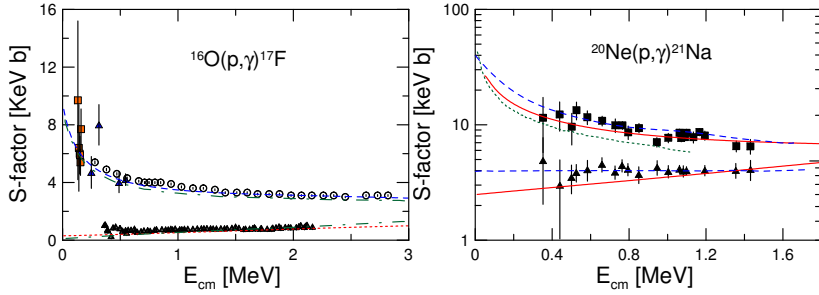


**FIGURE 7.** *Left.* Single-particle model calculation for the reaction  $^{16}\text{O}(p,\gamma)^{17}\text{F}$ . The dotted line and the dashed line are for the capture to the ground state and to the first excited state respectively. The experimental data are from Refs. [46, 47, 29, 48]. The dotted-dashed lines are the result of shell model calculations published in Ref. [49]. *Right.* Single-particle model calculation for the reaction  $^{20}\text{Ne}(p,\gamma)^{21}\text{Na}$ . Upper solid line is for the capture to the 2.425 MeV excited state of  $^{20}\text{Ne}$  and lower solid line for the 0.332 MeV excited state. Experimental data are from Ref. [50]. The dashed and dotted lines are theoretical results from Ref. [50] and Ref. [51], respectively

are relevant. It is worthwhile to mention that these arguments are reasonable for proton capture at very low energies, because of the Coulomb barrier.

As the overlap integral, Eq. 13, asymptotically becomes a Whittaker function, so does the single particle bound-state wavefunction  $u_\alpha$ , calculated with Eq. 4. If we call the single particle ANC by  $b_i$ , then the relation between the ANC obtained from experiment, or a microscopic model, with the single particle ANC is given by  $(SF)_i b_i^2 = C_i^2$ . This becomes clear from Eq. 9. The values of  $(SF)_i$  and  $b_i$  obtained with the simple potential model are useful telltales of the complex short-range many-body physics of radiative capture reactions [1].

Table 2 summarizes the potential parameters used in cases where the potential model works reasonably well for radiative proton capture reactions. In figures 1-7 we compare the calculated cross sections for radiative proton capture with the available experimental data. More calculations for neutron capture reactions can be found in Ref. [1]. The agreement with the experimental data is remarkable in view of the simplicity of the model.

## ACKNOWLEDGMENTS

This work was partially supported by the U.S. DOE grants DE-FG02-08ER41533 and DE-FC02-07ER41457 (UNEDF, SciDAC-2) and by the Research Corporation.

## REFERENCES

1. J. P. Huang, C. A. Bertulani and V. Guimarães, Atomic Data and Nuclear Data Tables, 2010.
2. G.M. Griffiths, E.A. Larson and L.P. Robertson, Can. J. Phys. 40, 402 (1962).
3. B.L. Berman, L.J. Koester Jr. and J.H. Smith, Phys. Rev. 133, B117 (1964).
4. W. Wolfli, R. Bosch, J. Lang, R. Muller, and P. Marmier, Helv. Phys. Acta 40, 946 (1967).

5. G.J. Schmid et al, Phys. Rev. C 52, R1732 (1995).
6. R. Bruss et al, in: F. Käppeler, K. Wisshak (Eds.), Proc. Nuclei in the Cosmos, Karlsruhe, Germany, 1992, IOP, 1993, p. 169.
7. Z.E. Switkowski et al, Nucl. Phys. A 331 (1979) 50.
8. K. Arai et al, Nucl. Phys. A 699 (2002) 963.
9. D. Zahnow et al, Z. Phys. A 351 229 (1995).
10. F. J. Vaughn, R. A. Chalmers, D. Kohler and L. F. Chase, Phys. Rev. C 2, 1657 (1970).
11. B. W. Filippone, A. J. Elwyn, C. N. Davids and D. D. Koetke, Phys. Rev. C 28, 2222 (1983).
12. L. T. Baby et al., Phys. Rev. Lett. 90, 022501 (2003).
13. A. R. Junghans et al, Phys. Rev. C 68, 065803 (2003).
14. N. Iwasa et al., Phys. Rev. Lett. 83, 2910 (1999); B. Davids et al., *ibid.* 86, 2750 (2001); F. Schumann et al., *ibid.* 90, 232501 (2003).
15. R.W. Kavanagh et al., Bull. Am. Phys. Soc. 14, 1209 (1969).
16. L. Trache et al, Phys. Rev. C 66, 035801 (2002).
17. D. Beaumel et al, Phys. Lett. B 514, 226 (2001).
18. P. Mohr, Phys. Rev. C 67, 065802 (2003).
19. D. Zahnow, C. Angulo, M. Junker, C. Rolfs, S. Schmidt, W. H. Schulte and E. Somorjai, Nucl. Phys. A 589, 95 (1995).
20. A. Sattarov et al, Phys. Rev. C 60, 035801 (1999).
21. Xiaodong Tang et al, Phys. Rev. C 67 015804 (2003).
22. C. Rolfs and R. E. Azuma, Nucl. Phys. A227, 291 (1974).
23. C. D. Nesaraja et al, Phys. Rev. C 64, 065804 (2001).
24. O. Camargo et al, Phys. Rev. C 78, 034605 (2008).
25. K. Miura et al, Nucl. Phys. A 539, 441 (1992).
26. A. Lefebvre et al., Nucl. Phys. A 592, 69 (1995).
27. Z. H. Li et al, Phys. Rev. C 74, 035801 (2006).
28. C. Rolfs, W. S. Rodney, Nucl. Phys. A 235 (1974) 450.
29. C. Rolfs, Nucl. Phys. A 217 (1973) 29.
30. J. D. King et al, Nucl. Phys. A567, 354 (1994).
31. Guo Bing, Li Zhi-hong, Chin. Phys. Lett. 24, 65 (2007).
32. A. Formicola et al, Phys. Lett. B 591 (2004) 61.
33. R. E. Pixley. The reaction cross section of nitrogen 14 for protons between 220 keV and 600 keV. Ph. D. Thesis, California Institute of Technology, 1957.
34. U. Schroeder et al, Nucl. Phys. A467 (1987) 240.
35. D. F. Hebbard, Nucl. Phys. 15 (1960) 289.
36. A. M. Mukhamedzhanov, P. Bem, V. Burjan et al, Phys. Rev. C 78, 015804 (2008).
37. Y. Nagai, et al., Phys. Rev. C 71, 055803 (2005).
38. R. Kanungo et al, Phys. Lett. B 660 (2008) 26.
39. Z.Q. Mao and A.E. Champagne, Nucl. Phys. A 522 (1991) 568.
40. M. B. Tsang, Jenny Lee and W. G. Lynch, Phys. Rev. Lett. 95, 222501 (2005).
41. F. Ajzenberg-Selove, Nucl. Phys. A 523, 1 (1991).
42. T. Kikuchi et al, Phys. Rev. C 57, 2724 (1998).
43. J. D. Goss et al., Phys. Rev. C 12, 1730 (1975).
44. W. Bohne et al, Nucl. Phys. A 196, 41 (1972).
45. J. Meissner et al, Phys. Rev. C 53, 459 (1996).
46. R. E. Hester, R. E. Pixley and W. A. Lamb, Phys. Rev. 111 1604 (1958).
47. N. Tanner, Phys. Rev. 114 1060 (1959).
48. R. Morlock, R. Kunz, A. Mayer et al, Phys. Rev. Lett. 79 3837 (1997).
49. K. Bennaceur et al, Phys. Lett. B 488, 75 (2000).
50. C. Rolfs, W.S. Rodney, M.H. Shapiro, and H. Winkler, Nucl. Phys. A 241, 460 (1975).
51. A. M. Mukhamedzhanov et al, Phys. Rev. C 73, 035806 (2006).